Saynisch, J., Semmling, M., Wickert, J., Thomas, M. (2015): Potential of space-borne GNSS reflectometry to constrain simulations of the ocean circulation. - *Ocean Dynamics*, *65*, 11, p. 1441-1460.

DOI: http://doi.org/10.1007/s10236-015-0886-y

Noname manuscript No.
(will be inserted by the editor)

Potential of space-borne GNSS reflectometry to constrain simulations of the ocean circulation

A case study for the South African current system

J. Saynisch · M. Semmling · J. Wickert · M. Thomas

the date of receipt and acceptance should be inserted later

Abstract The Agulhas current system transports warm and salty water masses from the Indian Ocean into the Southern Ocean and into the Atlantic. The transports impact past, present and future climate on local and global scales. The size and variability, however, of the respective transports are still much debated. In this study, an idealized model based twin experiment is used to study whether sea surface height (SSH) anomalies estimated from reflected signals of the Global Navigation Satellite System (GNSS-R) can be used to determine the internal water mass properties and transports of the Agulhas region. A space-borne GNSS-R detector on the International Space Station (ISS) is assumed and simulated. The detector is able to observe daily SSH fields with a spatial resolution of 1-5°. Depending on reflection geometry, the precision of a single SSH observation is estimated to reach 3 cm (20 cm) when the carrier phase (code delay) information of the reflected GNSS signal is used. The average precision over the Agulhas region is 7 cm (42 cm). The proposed GNSS-R measurements surpass the radar-based satellite altimetry missions in temporal and spatial resolution but are less precise. Using the estimated GNSS-R characteristics, measurements of SSH are generated by sampling a regional nested general circulation model of the South African oceans. The artificial observations are subsequently assimilated with a 4DVAR adjoint data assimilation method into the same ocean model but with a different initial state and forcing. The assimilated and the original, i.e., the sampled model state are compared to systematically identify improvements and degradations in the model variables that arise due to the assimilation of GNSS-R based SSH observations. We show that SSH and the independent, i.e., not assimilated model variables velocity, temperature and salinity improve by the assimilation of GNSS-R based SSH observations. After the assimilation of 90 days of SSH observations, improvements in the independent variables cover the whole water column. Locally, up to 39 % of the original model state are recovered. Shorter assimilation windows result in enhanced reproduction of the observed and assimilated SSH but are accompanied by an insufficient or wrong recovery of sub-surface water properties. The assimilation of real GNSS-R observations, when available, and consequently the estimation of Agulhas water mass properties and the leakage of heat and salt into the Atlantic will benefit from this model based study.

Keywords Agulhas current · data assimilation · GNSS reflectometry

J. Saynisch · M. Semmling · J. Wickert · M. Thomas
Helmholtz Centre Potsdam GFZ German Research Centre Potsdam, Germany. E-mail: saynisch@gfz-potsdam.de

M. Thomas
Freie Universität Berlin Institute of Meteorology, Berlin, Germany.

1 Introduction

The oceans around South Africa are dominated by the Agulhas current and the Agulhas Retroflection. At the retroflection the Agulhas reverses its zonal direction and flows as the Agulhas Return Current eastward parallel to the Antarctic circumpolar current (ACC). The regional implications of the Agulhas current system range from ecological to meteorological and impact the southern African continent. Furthermore, from the westernmost extension of the Agulhas current, large eddies are shed that leak heat and salt from the Indian Ocean into the Atlantic. These Agulhas rings travel northwest into the central and northern Atlantic and influence the Gulf Stream, the North Atlantic Current and finally the Atlantic meridional overturning circulation (Beal et al. 2011; Ruehs et al. 2013). By this tele-connection the South African current system has an important impact on past,

present and future climate (Weijer and van Sebille 2014; Koutsodendris et al. 2014). The strength and variability of the Agulhas system and the amount of leaked heat and salt are highly unknown (Beal et al. 2011). In-situ measurements are very sparse and satellite observations can only be used to derive the sub-surface transports when calibrated by dynamic ocean models or by the sparse in-situ measurements (Ivchenko et al. 2011; Sebille et al. 2010; Le Bars et al. 2014). Since initial and boundary conditions cannot be known with unlimited accuracy, even perfect models of a highly nonlinear system as the Agulhas/ACC region can reproduce the true state of the modelled system only to some degree. The less linear a system is, the more solutions satisfy the governing equations of the system (with the extremes being linearity and chaos). The rigorous combination of observations and models is necessary to distinguish the existing, i.e., the observable solution from the many physically possible. If this combination is done systematically, it is called data assimilation. Backeberg et al. (2014) use a basic data assimilation technique, the optimal interpolation, for such a systematic combination of satellite altimetry based sea surface height (SSH) observations and a nested ocean model of the Agulhas region, resulting in improved water mass properties and deep current velocities. Our paper has a similar approach but studies the potential of prospective space-borne GNSS-R based SSH observations to determine the internal water mass properties of the Agulhas region in an idealized, i.e., model-only scenario.

The use of GNSS reflectometry (GNSS-R) for ocean remote sensing has been investigated during the last two decades. GNSS-R estimates SSH by comparing the transit-times between GPS-satellite signals on the direct path and on the ocean reflected path. SSH measurements have already been reported for airborne experiments (Lowe et al. 2002; Ruffini et al. 2004; Rius et al. 2010; Semmling et al. 2014). A respective space-borne GNSS-R setup is expected to increase the global temporal and spatial resolution of ocean observations (Martin-Neira 1993; Wickert et al. 2009) as GNSS guarantees at least four simultaneous direct links between the GPS-satellites and the receiver. These observations with variable incidence provide a larger swath (cross-track observation range) compared to conventional radar altimeters operated on similar platforms. However, the currently expected accuracy of the GNSS-R measurements is less than that of conventional altimeters. In this study, a scenario is considered that comprises a single LEO satellite (the ISS) equipped with a GNSS-R receiver. The characteristics of this constellation are estimated and applied to sample modelled SSH from a reference simulation of the Agulhas region. Subsequently, the artificial SSH observations are assimilated with a state of the art 4DVAR adjoint method into the same model but into a simulation that differs by initial state and forcing. Consequently, the quality of the assimilation can be evaluated by the recovery of the reference simulation in the assimilated simulation.

The goal of this initial paper on assimilation of GNSS-R is to study the usability of GNSS-R based SSH measurements in the oceanographic context in principle. We investigate what oceanographic information can be drawn out of the envisioned space-borne measurements and where caution has to be applied. Furthermore, we study the requirements the data should fulfill, i.e., distinguish critical from negligible characteristics of GNSS-R measurements to aid the design choices for respective satellite missions.

The paper is structured as followed. The GNSS-R constellation, the measurement characteristics, the data assimilation method and the ocean model are described in Sec. 2. The setup of the twin model experiment and the sampling of characteristic GNSS-R observations of SSH is described in Sec. 3. The results of the experiments are presented and discussed in Sec. 4. We summarize the results in Sec. 5.

2 Methods and Data

2.1 Ocean models

The study is conducted by using the Regional Ocean Modeling System (ROMS, Shchepetkin and McWilliams 2003, 2005). ROMS is a free-surface, terrain-following, primitive equations ocean model. The modelled region extends from 57.5° S to 5° S and from 15° W to 55° E (see Fig. 2). The incorporated spatial resolution is 0.20° in latitude, 0.25° in longitude and 32 σ-layers in the vertical. The time step is 10 minutes for baroclinic processes and 40 seconds for barotropic processes. The regional model is forced with 6-hourly fields for wind stress, freshwater flux and heat flux from the ERA-Interim reanalysis of the European Centre for Medium-Range Weather Forecasts (ECMWF, Uppala et al. 2008). The regional ROMS model is nested in the global Ocean Model for Circulation and Tides (OMCT, Thomas et al. 2001). The OMCT generates daily boundary conditions for the ROMS model, i.e., velocities, temperatures (T), salinities (S) and sea surface heights (SSH) as described in Kuhlmann et al. (2013). Consistent with the regional model's forcing, the global model is forced with ERA-Interim data for heat flux, wind stress and freshwater flux, too.

2.2 Data assimilation

Data assimilation methods aim to minimize the misfit between models and observations in an optimal and systematic way. The data assimilation scheme used in this study is the incremental strong constraint four-dimensional variational method (IS4DVAR). The method, its implementation in ROMS and its performance are described in detail in

Moore et al. (2011a,b,c). The conjugate-gradient-like Lanczos approach is used to minimize a quadratic cost function which measures the model-to-observation misfit. In our application, Ritz preconditioning with 25 inner loops (i.e., 26 Lanczos vectors) and one outer loop are used (in the end of the paper examples for three outer loops are shown).

Since the IS4DVAR is a strong constraint method, only the initial state of the ROMS ocean model is allowed to change under the influence of the assimilated observations. In addition, the prescribed open boundary conditions from the OMCT ocean model are allowed to be adjusted by the IS4DVAR algorithm once per day. The same accounts for the prescribed atmospheric forcing fields from the ECMWF.

Since the model state in the assimilation experiment includes errors of the size of the seasonal cycle (see Sec. 3), the uncertainties of the model variables and the initial state are estimated by the standard deviation of an unconstrained ROMS model simulation over one year (2002). The uncertainties of the forcing and boundary conditions are estimated by the standard deviation of the forcing fields over the same year.

2.3 GNSS-R Data

Reflectometry Simulation

A GNSS-R receiver operating on the ISS orbit is considered for this study. Referring to Wickert et al. (2009), the ISS is expected to be a suitable LEO platform for space-borne GNSS-R. The simulation regards all available GPS satellites. Specular reflection points are found on a modelled surface using given receiver and transmitter positions. Computation obeys the reflection law, i.e., incidence angle (ϕ) and reflection angle at the specular point are equal. The nadir angle of reflection θ at the receiver is additionally defined to characterize the field of view, see small plot of Fig. 1. Broadcast GPS ephemerides data and NORAD two line elements of the ISS are used for transmitter and receiver positioning, respectively. The surface model accounts for an ellipsoidal Earth (WGS-84) in spherical approximation as described in Semmling (2012). Signal refraction in the troposphere and the ionosphere is disregarded. Example results of specular point calculation including kinetics of transmitters and the receiver are shown in Fig. 1. The specular tracks run almost parallel to the receiver tracks. The reason is the short distance of the specular point to the ISS-based receiver compared to the transmitter distance. The rather high ISS angular velocity, which is proportional to the orbit number in Tab. 1, leads to comparable velocities of the specular point. The example track of PRN 21 in Fig. 1 illustrates the increased swath if reflections from distant transmitters with high nadir angles ($\theta = 57^\circ$) are observed. Reflections considered in this simulation are limited to $\theta < 67^\circ$. This limit corresponds to a maximum swath of about 3000 km. For practical application, however, a reduced swath must be considered, due to limitations in the field of view and the antenna gain, which are disregarded here. Altogether, reflection events for two days are simulated in this study comprising almost 31 ISS orbits. The resulting reflection track density is much higher than for single-satellite altimeter missions (e.g., Envisat, 30 days repeat-cycle with 431 orbits per cycle, Pujol et al. (2012)). The biggest zonal respectively meridional gaps of the calculated daily fields reach up to 10° but the average resolution over the Agulhas region is below 0.5° (see Fig. 2, left panel).

	GPS	ISS
orbit height [km above sea level]	20200	420
orbit number [per day]	2.006	15.484
orbit inclination [°]	55	52
orbit planes/sat. in plane	6/4	1/1

Table 1 Orbit characteristics of transmitters aboard GPS satellites and the receiver aboard ISS.

Precision of Reflection Events

A challenge in today's ocean altimetry is the resolution of eddy-scale ocean topography (Bosch et al. 2012). The improved resolution of recent Earth gravity field models (e.g., due to data from the GOCE mission) yields 5 cm precision in SSH (Albertella et al. 2012). Such a precision is challenging for GNSS-R retrievals. Different altimetric retrievals have been described for airborne GNSS-R experiments. In the following we distinguish between code delay observations (Lowe et al. 2002; Rius et al. 2010; Carreno-Luengo et al. 2013) and carrier phase observations (Semmling et al. 2014). In general, the code delay has a coarser precision compared to the carrier phase. The simulation uses an altimetric precision $\hat{\delta}_{code}$ of 20 cm based on code delay retrieval as given by Cardellach and Rius (2008). This precision is anticipated for the GEROS-ISS mission and a rather conservative assumption compared to precisions reported for recent airborne experiments (Carreno-Luengo et al. 2013; Semmling et al. 2014). Therefore, a precision $\hat{\delta}_{phase}$ of 3 cm for carrier phase retrieval, based on observations described in Semmling et al. (2014) is used in addition. The value $\hat{\delta}$ is the best precision, respectively. It assumes the highest altimetric sensitivity $\frac{\Delta p}{\Delta H}$ which is the ratio of signal path changes Δp induced by a height shift ΔH of the reflecting surface and is computed by two runs of the ray tracing tool for different reflection heights. The sensitivity and the derived precision $\delta = \frac{\Delta p}{\Delta H}\hat{\delta}$ vary with the angle of reflection incidence, as shown for the example events in Tab. 2. Best precision results from nadir incidence ($\theta = 0^\circ$) where the sensitivity is 2 (see PRN 5). It decreases at smaller incidence angles where the sensitivity falls below 1 (see PRN 21). The

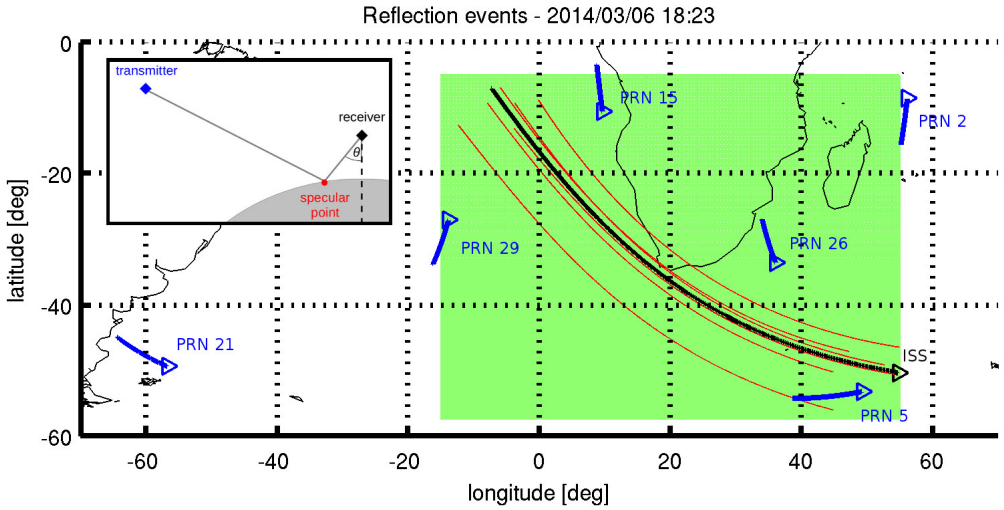

Fig. 1 Track location of transmitters (blue), receiver (black) and specular points (red). A constellation example is shown with the ISS based receiver passing over the area of interest (green). Small plot: Scheme of reflection geometry including the nadir angle θ.

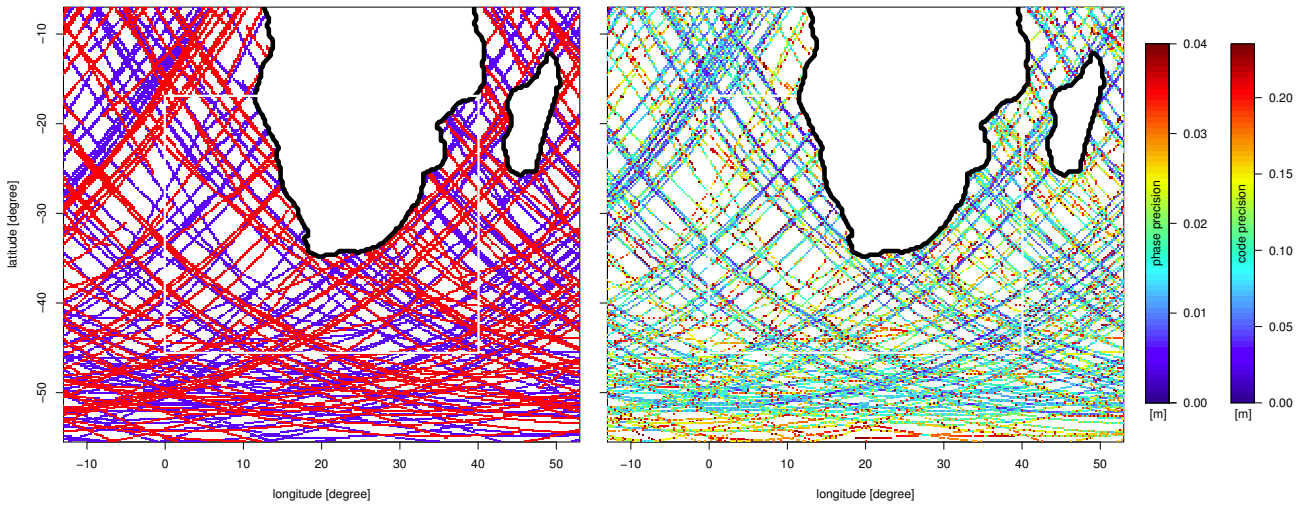

Fig. 2 Configuration of the artificial SSH observations by GNSS reflectometry. Left: GPS satellite reflection ground-tracks of two consecutive days (blue, red). Right: Precision at the respective grid-point, i.e., precision of the single measurements divided by the number of observations. Modelled SSH data is collected within the white rectangle only.

resulting phase (code) based precisions of single SSH observations have a range of 3-16 cm (20-92 cm) and a mean precision of 7 cm (42 cm). Divided by the number of SSH observations for every grid point the finally utilized precisions arise, see Fig. 2 (right panel). During one day, every ocean model grid point is sampled by zero or one GNSS-R measurement, but a few grid points have multiple measurements of up to 23 observations per day.

This simulation study only considers precision. Statements on the altimetric accuracy are postponed, as further investigations are required to study biases, for example introduced by tropospheric and ionospheric refraction.

3 Experiment setup

The experiment setup is depicted in Fig. 3. The South African oceans are simulated with ROMS for the year 2002. Snapshots of the model state, i.e., velocity, density, S, T and SSH are stored once per day. This simulation represents the true state or truth of the twin experiment and will be called TRUTH hereafter. To generate SSH observations, the SSH of TRUTH are collected on the GNSS-R reflection tracks described in Sec. 2.3. The reflection tracks of the two different satellite constellation-days represent typical measurement days and are used in alternating sequence to account for the stochas-

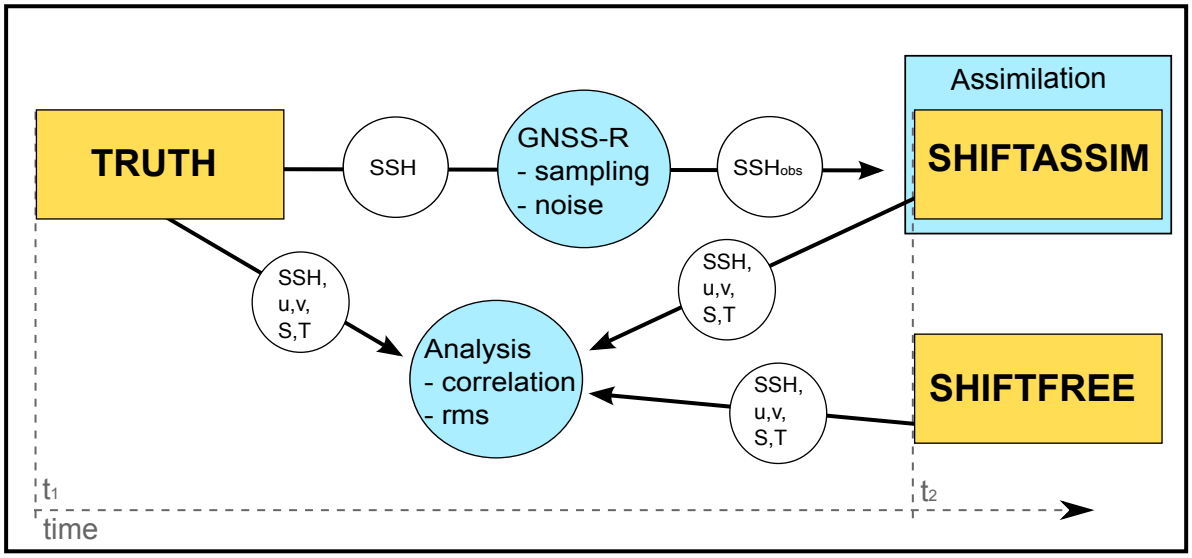

Fig. 3 Schematic of the experiment setup. Yellow boxes: ocean model simulations. White circles: provided data. Blue: operators.

PRN	θ [deg]	$\Delta p/\Delta H$ [m/m]	δ_{code} [cm]	δ_{phase} [cm]
5	4	2.0	20	3
26	13	1.9	21	4
15	16	1.9	21	4
29	23	1.8	22	4
2	42	1.4	28	5
21	57	0.9	45	8

Table 2 Compared precisions of the examples of reflection events shown in Fig. 1. Best precision within each event are given. The smallest nadir angle θ (see Fig. 1) corresponds to the highest sensitivity $\Delta p/\Delta H$ and best precision values δ, respectively.

tic distribution of the tracks. Every SSH value acquired this way is additively scrambled with Gaussian noise of standard deviation equal to the precisions described in Sec. 2.3. In correspondence to the alternating sampling pattern, the precisions of the two different satellite constellation-days are used in alternating sequence. The sampling process is repeated for code-precision and for phase-precision. The results are two gappy fields of noisy SSH observations for every day of 2002, one with code-precision and one with phase-precision.

The artificial SSH observations together with the respective precision information for every day and every grid point are assimilated with the ROMS model. For evaluation purposes (see Sec. 4), the SSH observations are assimilated only in a fraction of the South African model domain (see white rectangle in Fig. 2).

The assimilation period starts at 1st July 2002, i.e., six month later than when the SSH observations are sampled from TRUTH. The two periods are maximally out of phase with respect to the seasonal cycle and the resulting deviations have to be considered in the assimilation error budget (see Sec. 2.2). Because of the time shift, the assimilation experiment is called SHIFTASSIM from now on. This setup is a classical twin experiment where the two simulations differ by forcing and initial conditions (cf. Fig. 3). The setup mimics the common situation where real observation data is assimilated in an ocean model and model state and forcing deviate from the real state and the size of these deviations are unknown. In contrast to this real world situation, the described twin experiment setup provides the true ocean state trajectory, the true forcing and in addition, the true noise free observations. Consequently, the quality of the assimilation is evaluated by the retrieval of the TRUTH model state in the SHIFTASSIM simulation by using the SSH observations of TRUTH.

With this setup, 36 assimilation experiments are conducted. Each experiment differs in one of the following characteristics from all the others: assimilation window length (30, 60 or 90 days), shift of the assimilation window with respect to 1st July 2002 (0, 30 or 60 days), allowed or forbidden adaptation of the atmospheric forcing by the assimilation, and using SSH observations of phase- or code-precision. Note that the number of necessary assimilation experiments in combination with the CPU-h and memory consumption of 4DVAR limits the window length of the study to 90 days. A single 90 days assimilation uses 60 GB memory on a 64 CPU supercomputer for 75 hours. The ROMS model in the used configuration (see Sec. 2.1) is eddy permitting. The data assimilation with an eddy resolving model would be more challenging and computationally much more demanding.

In contrast to conventional nadir looking altimeters, GNSS-R measurements allow a wide range of incidence angles. Especially large incidence angles ($\phi \geq 40°$) increase the cross track ocean coverage. Those measurements, however, differ particularly from conventional altimetric measurements

and are insufficiently studied so far. Airborne experiments proved GNSS-R based SSH retrievals also at large incidence angles (Semmling et al. 2014). However, dependent on the incidence angle the retrievals are affected by sea surface roughness. To account for these effects, some of the SHIFTASSIM have been repeated by using only observations with reflection incidence angles $\phi \leq 40^\circ$ (c.f., Sec. 2.3). In addition, selected SHIFTASSIM have been repeated with a higher number of outer loops (c.f., Sec. 2.2).

To separate the influence of the SSH data assimilation from the similarities that TRUTH and a 6 month shifted simulation may have naturally, a control simulation is calculated which consists of a free forward simulation that starts at 1st July 2002, i.e., like SHIFTASSIM. This simulation is not constrained by any observations. It is called SHIFTFREE from now on (see Fig. 3). Note, in an eddy resolving configuration the resemblance between TRUTH and SHIFTASSIM respectively SHIFTFREE would both be smaller but the conclusions drawn from their inter-comparison would still be similar.

4 Results and Conclusions

Fig. 4 shows the root-mean-square (rms) misfits between SSH from SHIFTASSIM respectively SHIFTFREE and the true observations, i.e., the noise-free SSH of TRUTH averaged over the assimilation area (Fig. 2, white rectangle). For better overview, not all of the SHIFTASSIM experiments (see Sec. 3) are plotted. The rms of the SHIFTFREE describe the differences that arise due to the six-month time shift between the two unconstrained simulations. The SHIFTFREE differences to TRUTH, i.e., the black circles range between 32-38 cm and have a mean of 35 cm. The respective differences to TRUTH arise from SHIFTFREE's different initial ocean state in combination with the different atmospheric forcing. The rms of all SHIFTASSIM experiments are smaller than the SHIFTFREE rms. We conclude that the assimilation is working on the technical level.

The SHIFTASSIM rms reduction depends primarily on the length of the assimilation window. The 90 days SHIFTASSIM which starts at 1st July 2002 and allows the forcing to be adapted by the assimilation process (solid blue line) shows rms between 29-33 cm with a mean of 31 cm. The 60 days and 30 days SHIFTASSIM show an rms range of 26-30 cm and 23-26 cm with a mean of 28 cm and 24 cm. This corresponds to rms reductions of 4-17 %, 10-27 % and 23-36 % for the 90, 60 and 30 days SHIFTASSIM as referenced to the SHIFTFREE rms. The shifted assimilations which start 1st August respectively 1st September show only slightly different performances compared to the assimilations that start 1st July. We conclude that the assimilation is not sensitive to the particular day the assimilation starts and that the skill of the assimilation with respect to SSH recovery is dominated by the assimilations window length, it improves with shorter assimilation time windows.

The direct comparison of SHIFTFREE and SHIFTASSIM rms shows that the success in reproducing the true SSH varies over the model time steps. The temporal progression of the rms is not identical. Remember that the rms of SHIFTFREE originate in the experiment's design. The larger SSH deviations are more easily removed by the assimilation method and the SHIFTASSIM rms show a flatter temporal progression than the SHIFTFREE rms. The assimilation induced rms leveling is the more pronounced the shorter the assimilation window is, i.e., the 90 days SHIFTASSIM rms resemble more the SHIFTFREE rms than than the 30 days SHIFTASSIM rms. Since data assimilation is in general directly driven by the model to observation misfit (e.g., Le Dimet and Talagrand 1986; Evensen 1994), this rms leveling is typical when the temporal variations in the observation and model state error budgets are smaller than the variations in the model to observation misfits.

Since the IS4DVAR is a strong constraint method, i.e., assumes a perfect model, the rms reduction of the SHIFTASSIM simulations can only be achieved by an optimized initial state or by adjusted boundary conditions like the atmospheric forcing. To distinguish these influences on the reproduction of the true SSH, the assimilations are conducted with and without adjustment of the forcing. The SHIFTASSIM without forcing adjustment are plotted in Fig. 4 (dashed lines). For a better overview, only the non forcing adapting SHIFTASSIM which start 1st July are plotted. The comparison of dashed and solid lines shows that the adjustment of the forcing has a small effect on the SSH rms. The effect of the forcing adjustment is not entirely positive or negative over the respective assimilation window length. Integration of the rms over the respective assimilation windows shows a negative influence of the forcing adaptation on the rms reduction. We conclude that the forcing is not the main driving behind the the assimilation induced SSH adjustments and consequently not the main driving behind region's dynamics (cf. e.g., Pilo et al. 2015). Note, that other parameters like local bathymetry, coriolis force and gravity strongly influence the eddy propagation and the SSH, but these parameters are well known and are not allowed to change by the data assimilation. Therefore, the SSH adjustments are governed by internal water mass properties which are mainly a consequence of the assimilation's impact on the initial state of the ocean model. Therefore, shorter assimilation windows allow for a better SSH reproduction since the ocean system's memory loss is smaller on shorter time scales. This is not the only reason for the better SSH reproduction of short assimilation window length. In the 30 days SHIFTASSIM the amount of SSH observations to fit is only half respectively one third that of the 60 respectively 90 days

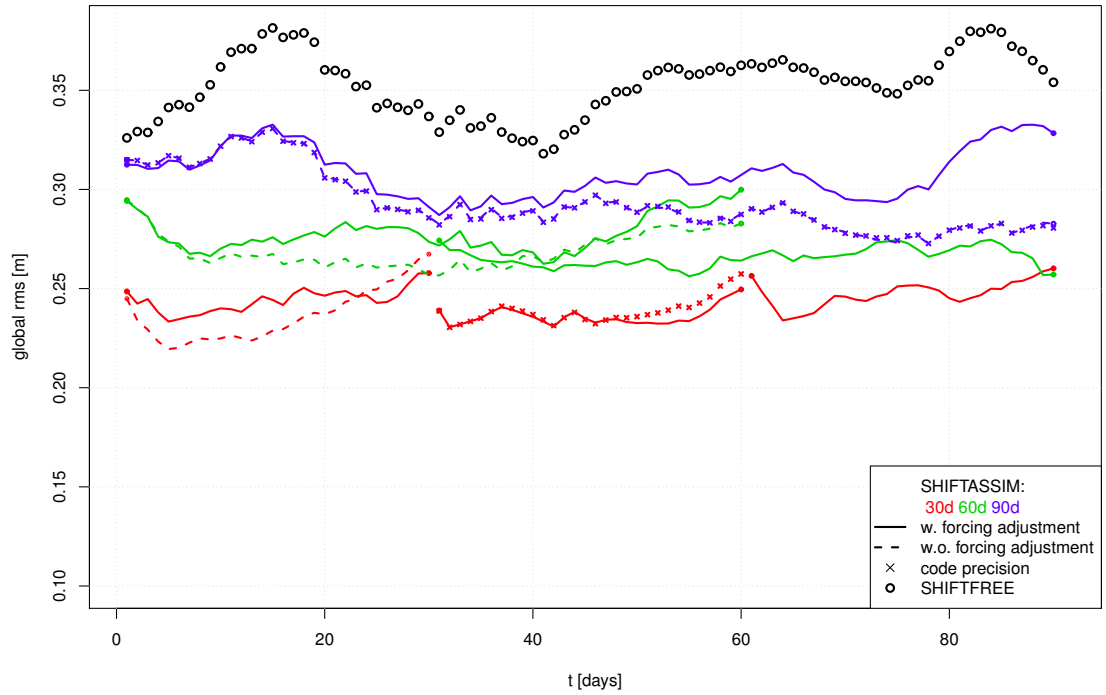

Fig. 4 Global mean rms misfits between SSH from SHIFTASSIM respectively SHIFTFREE and the true SSH (i.e., the noise-free SSH from TRUTH).

SHIFTASSIM and the assimilation's cost function is integrated over less data. Consequently, the assimilation's success per time step is bigger in contrast to the longer assimilation windows where the assimilation's success is smaller but spread over more time steps.

To study the influence of the precision and the signal-to-noise ratio of the assimilated SSH data, the SHIFTASSIM use SSH observations that are sampled with phase-precision and code-precision (see Sec. 3). Note, phase-precision is approximately six times more precise than code-precision (see Sec. 2.3). Again, without restriction of the general statement, the SHIFTASSIM that use code-precision (crosses) are plotted for selected cases only. The depicted 30 day SHIFTASSIM that assimilates SSH of code-precision allows the adjustment of the forcing and the depicted 90 day SHIFTASSIM forbids the adjustment of the forcing. The differences between the crosses and the respective (solid or dashed) lines are representative for the very small influence of the two different precisions and corresponding noise-levels of the SSH data, e.g., the differences between the two 30 day SHIFTASSIM which start in August have a maximum of 8 mm and a mean of 2 mm. We conclude that the region's governing processes in combination with the processes modelled in ROMS are sufficiently resolved by both, code and phase precision. The assimilation's high tolerance towards accuracy must consequently be attributed to the sufficiently high temporal and spatial resolution of GNSS-R observations which compensate for less accurate data.

Fig. 5 and Fig. 6 show the local contributions to the rms in Fig. 4. In Fig. 5 the differences between the temporal mean SSH from SHIFTFREE respectively SHIFTASSIM and TRUTH are plotted for different assimilation window lengths. In Fig. 6 temporal correlations between SSH from SHIFTFREE respectively SHIFTASSIM and TRUTH are plotted for different assimilation window lengths. Since Fig. 4 shows, that the performance of SHIFTFREE depends on the window length over which the correlation and the mean are calculated, the changes in the SHIFTASSIM have to be evaluated in comparison to the corresponding period of SHIFTFREE which are plotted for this purpose in the left panels. Because the plots from phase- and code-precision SHIFTASSIM and from disabled or allowed forcing adjustment are visibly indistinguishable, only phase-precision SHIFTASSIM with forcing adjustments are plotted as examples. Fig. 5 and Fig. 6 show again that the results primarily depend on the assimilation window length. Compared to the respective SHIFTFREE fields, the assimilations with shorter window length improve most, i.e., the differences between left and right panel are most pronounced in the top row of the figures. In all assimilations, the improvements are not restricted to the area where the SSH are assimilated (the white rectangle). Throughout the modelled region, differences in

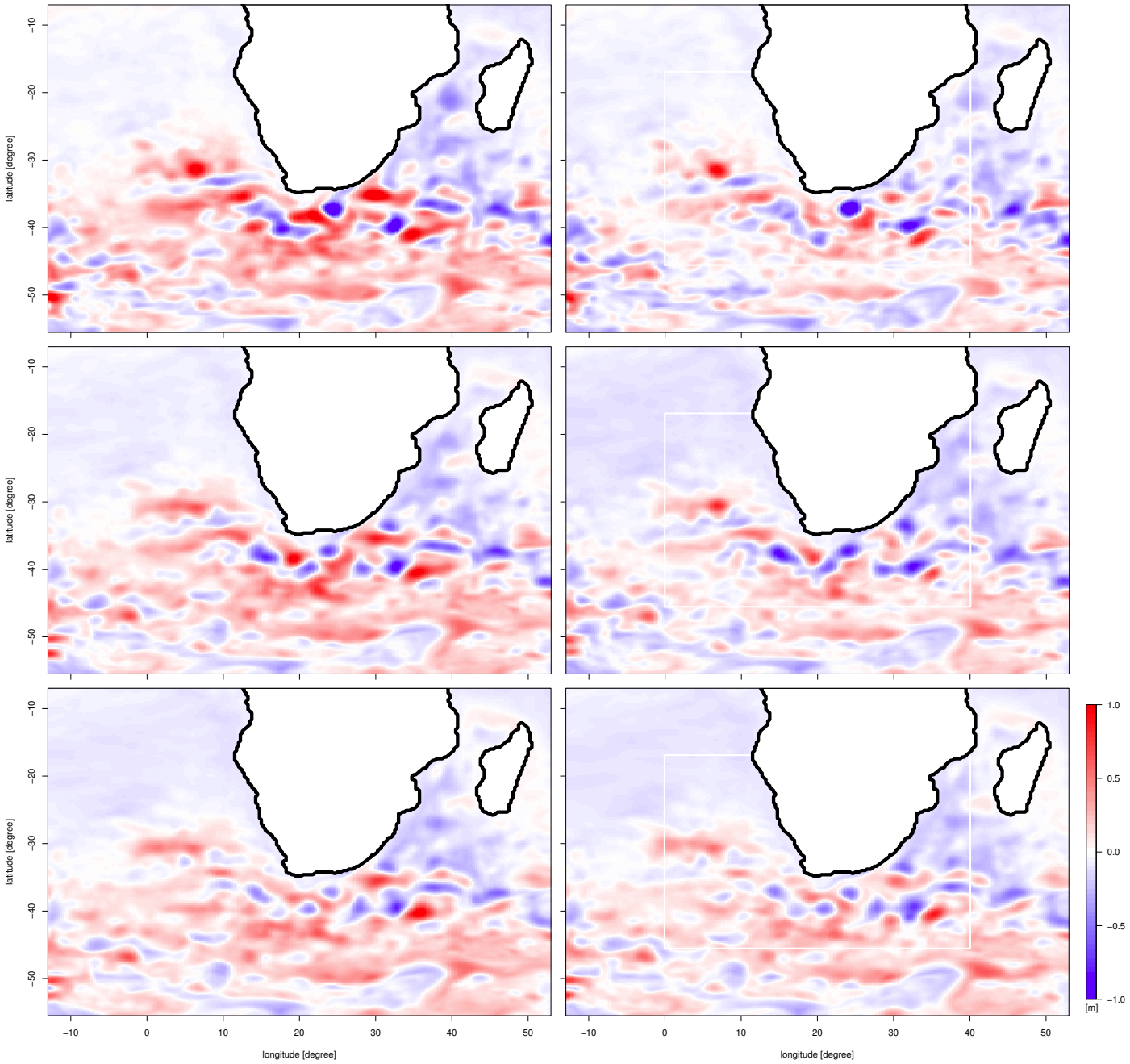

Fig. 5 Differences between mean true SSH (i.e., the mean noise-free SSH from TRUTH) and the mean SSH from SHIFTFREE (left side) respectively SHIFTASSIM (right side). From top to bottom: 30 days, 60 days, 90 days assimilation window length with forcing adjustment and phase precision. Data is assimilated within the white rectangle only.

mean SSH are reduced, correlations are strengthened and anticorrelations are reduced in strength and pattern-size. For example, compared to TRUTH, the rms misfits of the mean SSH fields for the 30 days SHIFTASSIM which starts at 1st July 2002 is 19 cm (Fig. 5, top-right). In the same period the SHIFTFREE has a mean SSH field with an rms misfit of 30 cm (Fig. 5, top-left). The rms improvement in the SSH mean field amounts to 11 cm.

Especially strong correlation improvements occur in the Benguela current system and the dynamically linked regions of the tropical Atlantic, i.e., regions where the flow points out of the assimilation area. This is an advantage of data assimilation with numerical ocean models over methods that base entirely on statistical information. Regions where the dominating flow points into the assimilation area also improve, but to a smaller extent.

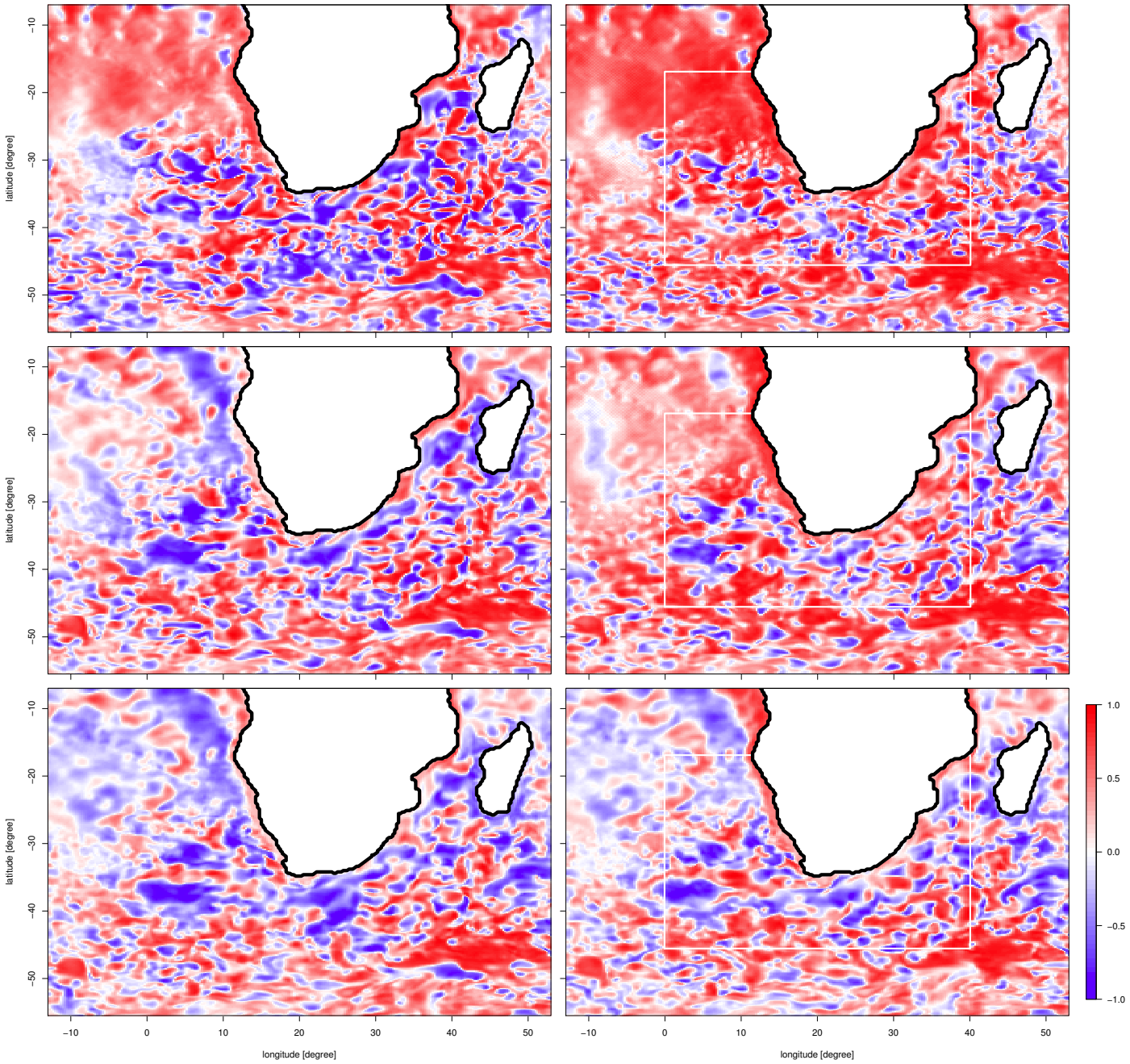

Fig. 6 Correlation between the true SSH (i.e., the noise-free SSH from TRUTH) and SSH from SHIFTFREE (left side) respectively SHIFTASSIM (right side). From top to bottom: 30 days, 60 days, 90 days assimilation window length with forcing adjustment and phase precision. Data is assimilated within the white rectangle only.

To evaluate the impact of the mean SSH and the SSH anomalies on the rms in Fig. 4 the temporal mean at every grid-point was removed and the remaining rms are calculated and plotted in Fig. 7 (dashed lines). The remaining improvements in the plotted period have a temporal average of 4 cm and must be attributed to improved temporal behavior in the SHIFTASSIM. Consequently, the average 11 cm of total rms reduction of the SHIFTASSIM over SHIFTFREE in Fig. 7 must be attributed to improvements in mean field and temporal behavior of SSH alike. The statement applies to all SHIFTASSIM (not explicitely shown).

The twin experiment configuration allows to study the impact of the assimilation of GNSS-R based SSH on dynamically linked but not directly constrained quantities, e.g., ocean water velocity, S, T and density. The rms misfits of these quantities with respect to TRUTH are calculated. Since

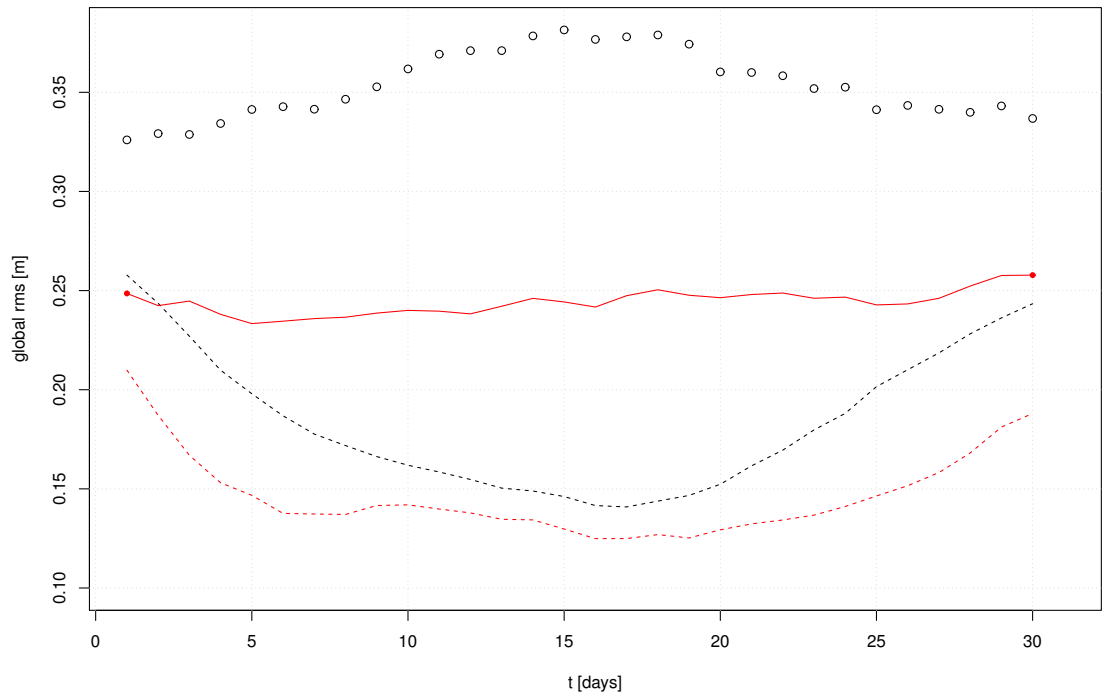

Fig. 7 Global mean rms misfits between SSH from SHIFTASSIM respectively SHIFTFREE and the true SSH (i.e., the noise-free SSH from TRUTH). Black: from SHIFTFREE. Red: from SHIFTASSIM. Dotted lines: rms misfits after removing the temporal mean at every grid point. Black circles and solid red line are the same as in Fig. 4.

TRUTH and the SHIFT simulations are maximally out of the annual phase, it is not expected to recover the entire three dimensional dynamical state of TRUTH by assimilating SSH observations for a few days. Nonetheless, SHIFTASSIM should show improvements in these quantities or at least no higher rms misfits than SHIFTFREE, i.e., the SHIFTASSIM must not show improvements in SSH which are generated by the wrong physical processes. Fig. 8 shows the changes in the rms misfit of velocities, T and S that arise due to the SSH assimilation, i.e., the rms misfits from SHIFTFREE minus the rms misfits from SHIFTASSIM. Positive values indicate smaller rms in SHIFTASSIM and therefore a better reproduction of TRUTH by SHIFTASSIM than by SHIFTFREE. Negative values indicate the opposite. First, the SHIFTASSIM of the 30 days assimilation window length are plotted with and without allowed forcing adaptation. The SSH assimilation impacts the whole three dimensional model space inside and outside of the assimilation region (between the vertical white lines). For T and S the impact is dominant in the upper ocean above 1000 m. The changes in SHIFTASSIM T and S are small (0.4 K, 0.02 psu) and not clearly closer or further away from TRUTH. The changes in SHIFTASSIM velocities behave very differently. The changes are dominant throughout the entire water column and peak inside the assimilation region. Unambiguously, the SHIFTASSIM velocities are further away from TRUTH than the SHIFTFREE velocities. This means, that the better SSH reproduction in SHIFTASSIM comes with the cost of lesser reproduction of sub-surface processes, i.e., the SSH improvements are realized by the wrong physical processes. The comparison of left and right panel of Fig. 8 shows that the deviations from TRUTH become larger when the assimilation is allowed to adjust the forcing. In general, divergent and convergent wind-stress will lead to sea level anomalies but in the Agulhas system where the SSH is governed by the current path and the propagating Agulhas rings, this is not the main physical mechanism behind the observed SSH. We conclude that in a real-world application the assimilation should be guided by assimilation of additional sub-surface velocity data. If sub-surface data is not available or reliable, the assimilation should be prevented from changing the wind-stress forcing.

Fig. 9 (left panel) shows the temporal development of the zonal velocity's rms misfit for the 30, 60 and 90 days SHIFTASSIM. In all cases, the largest misfits (negative pattern) appear in the beginning of the assimilation period in depths of 500-4500 m. Misfits of up to 10 cm/s occur. The misfits are stronger for shorter assimilation window length and decay over the first 20-25 days. Improved velocities (positive pattern) occur in the upper ocean (above 1000 m) from day 5 on

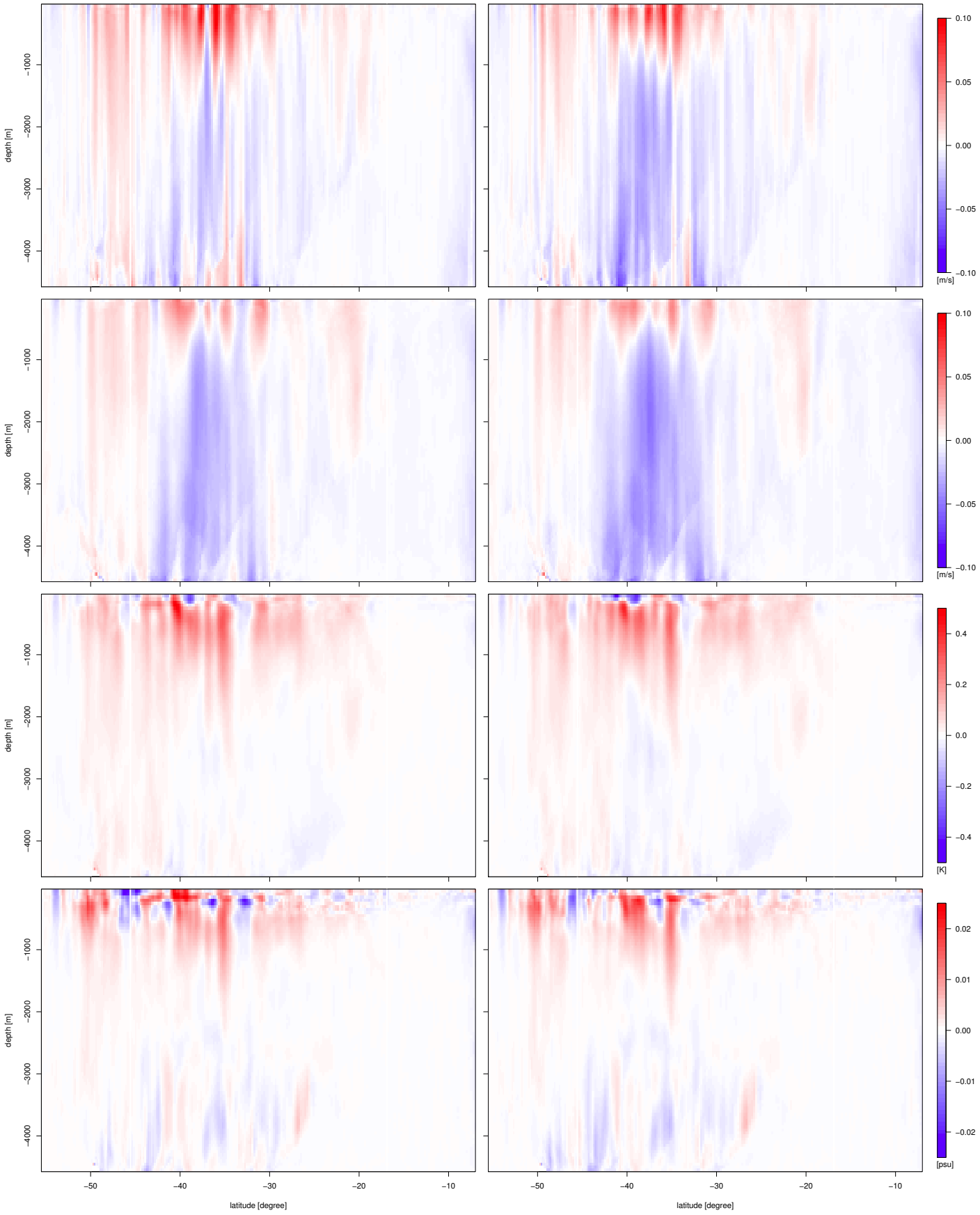

Fig. 8 Change in rms misfit due to SSH assimilation (i.e., differences between rms misfit of SHIFTFREE and SHIFTASSIM). Positive values indicate a better reproduction of the respective TRUTH quantities in SHIFTASSIM than in SHIFTFREE. Negative values state opposite. Zonal and temporal mean of the 30 days SHIFTASSIM which starts at 1st July 2002. SSH data is assimilated within the white bars only. From top to bottom: zonal velocity, meridional velocity, temperature, salinity. Left: Without forcing adaptation. Right: With forcing adaptation.

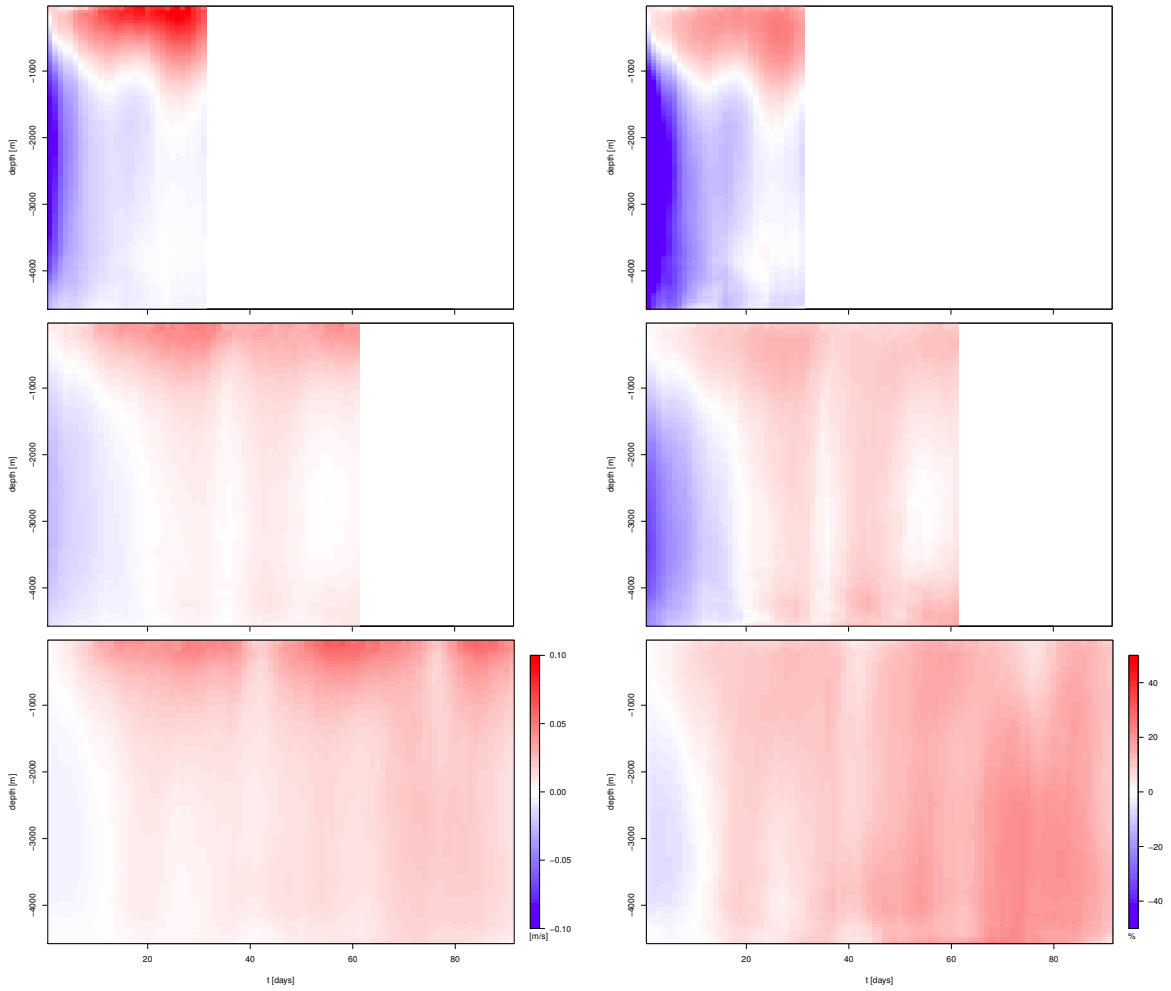

Fig. 9 Temporal development of the SSH assimilation impact on zonal velocity. Left panel: Differences between rms of SHIFTFREE and rms of SHIFTASSIM. Right panel: Differences between rms of SHIFTFREE and rms of SHIFTASSIM in relation to rms of SHIFTFREE. Positive values indicate a better reproduction of the respective TRUTH quantities in SHIFTASSIM than in SHIFTFREE. Negative values state the opposite. Horizontal mean for every time step and depth. Adaptation of the forcing is not allowed. From top to bottom: 30 days, 60 days, 90 days assimilation window length with phase precision and without forcing adjustment.

and grow in strength and depth. The improvements reach 10 cm/s, too. Although locally the improvements are stronger for the shortest assimilation window length, in the 60 and 90 days SHIFTASSIM the improvements cover the entire water column after 20-25 days, stating that from that time on the improved reproduction of the true SSH is realized by the true physical process. The choice of phase or code precision does not have a distinguishable impact on the reproduction of the water mass properties (not shown).

In relation to the deviations SHIFTFREE has by design from the TRUTH (Fig. 9, right panel), the zonal velocity of SHIFTASSIM improves up to 25 % in the case of the 30 days SHIFTASSIM. The maximum improvements are located in the upper ocean. The respective misfits in the beginning of the assimilation windows reach 100 % in the 30 days assimilation, i.e., the 30 days SHIFTASSIM velocity is initially twice as far away from TRUTH than SHIFTFREE. In the 60 days SHIFTASSIM the initial misfits amount to 35 % of that of SHIFTFREE and the maximal improvements amount to 20 %. The 90 days SHIFTASSIM has very small initial misfits of 7 % and improvements of up to 27 %. Improvements cover the entire water column for 80 days of the assimilation time window. The maximum is located at the ocean bottom in the second half of the assimilation window. The assimilation impact on meridional velocity is similar to the impact on the zonal velocity (Fig. 10), but substantial improvements are restricted to the 90 days SHIFTASSIM where the initial misfits are 6 % (same as for zonal velocity) and improvements reach 33 % (3 % larger than for zonal velocity).

The assimilation impact on S and T are summarized in Fig. 11 (note, that only the relative rms are plotted). The misfits to TRUTH are strongest in the 30 days SHIFTASSIM. The salinity (temperature) performs up to 28 % (62 %) worse

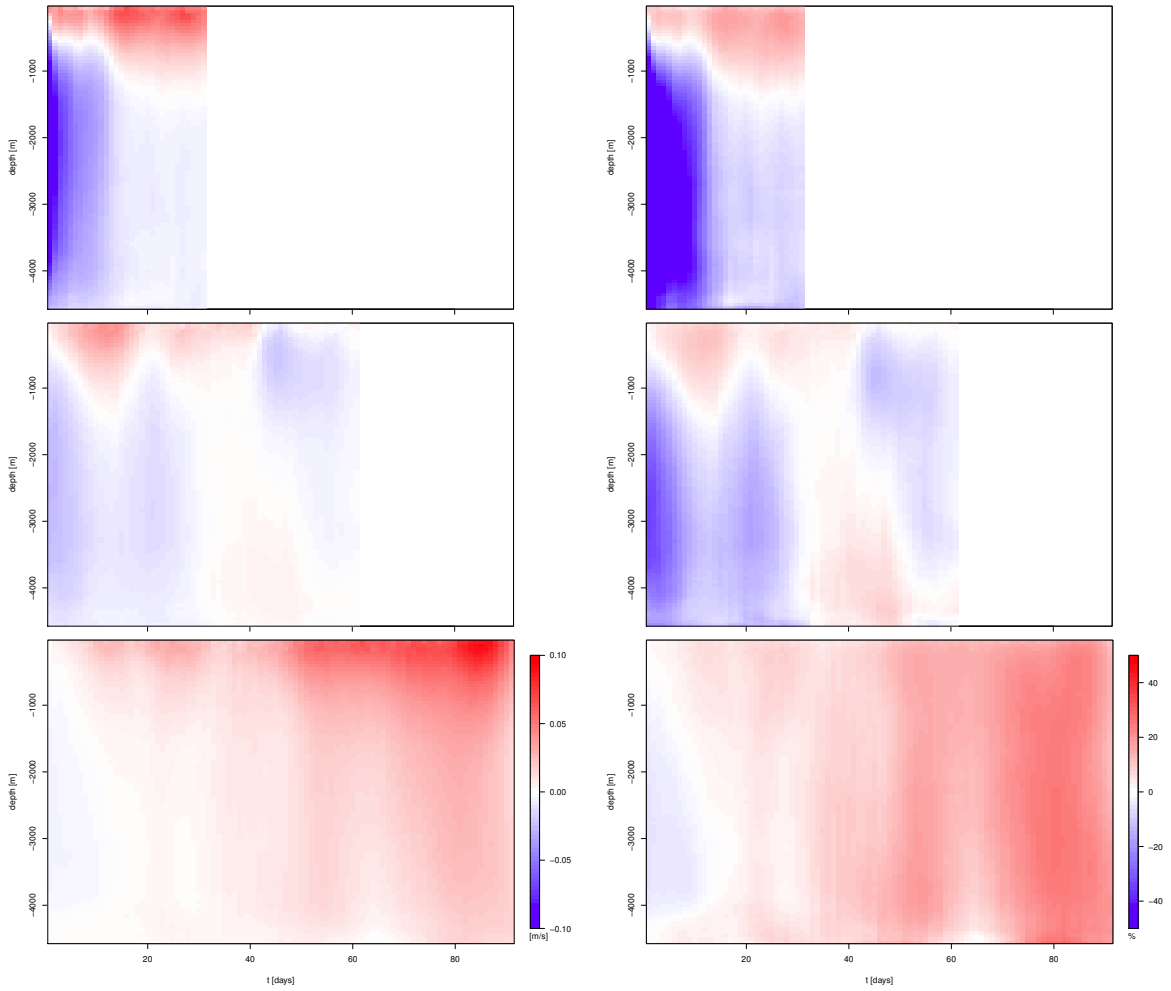

Fig. 10 Temporal development of SSH assimilation impact on meridional velocity. Left panel: Differences between rms of SHIFTFREE and rms of SHIFTASSIM. Right panel: Differences between rms of SHIFTFREE and rms of SHIFTASSIM in relation to rms of SHIFTFREE. Positive values indicate a better reproduction of the respective TRUTH quantities in SHIFTASSIM than in SHIFTFREE. Negative values state the opposite. Horizontal mean for every time step and depth. Adaptation of the forcing is not allowed. From top to bottom: 30 days, 60 days, 90 days assimilation window length with phase precision and without forcing adjustment.

than the SHIFTFREE simulation. Improvements grow in size and depth towards the end of the assimilation window and reach 25 % (28 %). Good results are visible for the 90 days SHIFTASSIM. Here, the maximum misfits in S (T) amount to 3 % (2 %) and the improvements cover the majority of time and space and reach values of 19 % (22 %). In physical units, the assimilation induced changes remain below 0.01 psu and 0.3 K in the 90 days SHIFTASSIM and the biggest changes are located above 1500 m (cf., Backeberg et al. (2014)). Compared to the velocities, the S and T changes are located 500 m deeper and do not start at the ocean surface (e.g., compare Fig. 10, right panel, and Fig. 11). In addition, the relative improvements in S and T are less homogenous throughout the water column than the improvements of the velocities. Especially, centered around 3000 m there is a water mass where S and T do not improve as much from the SSH assimilation as the water masses below and above. The SHIFTASSIM with forcing adaptation show the same temporal development and depth structure as the SHIFTASSIM without forcing adaptation but the improvements are only half as large (not shown).

For efficency, all previous results are acquired with a single outer loop in the assimilation procedure. After the characterization of the assimilation's impact on the ocean model trajectory, the success of the assimilation can further be risen by increasing the number outer loops.

Note, that the CPU-h consumption is approximately linear in the number of outer loops. Fig. 12 shows the temporal rms development of the independent water mass properties (u, v, S, T) after the assimilation with 3 outer loops (again, only the relative rms differences are plotted). The 30 days SHIFTASSIM improves by raising the number of outer loops (Fig. 12, left panel). The maximal horizontal mean initial misfits of internal water mass properties de-

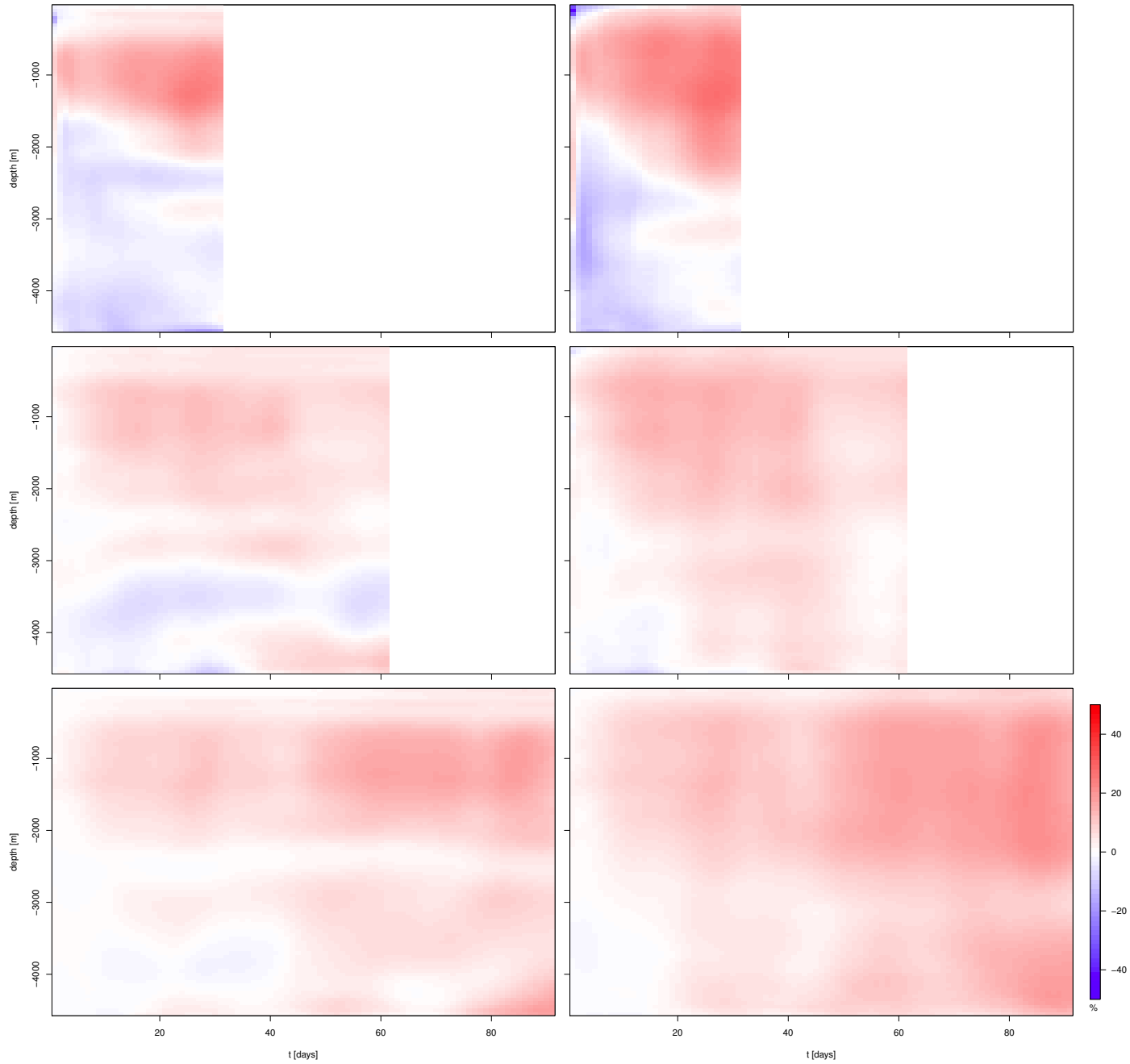

Fig. 11 Temporal development of the SSH assimilation impact on salinity (left panel) and temperature (right panel). Differences between rms of SHIFTFREE and rms of SHIFTASSIM in relation to rms of SHIFTFREE. Positive values indicate a better reproduction of the respective TRUTH quantities in SHIFTASSIM than in SHIFTFREE. Negative values state the opposite. Horizontal mean for every time step and depth. Adaptation of the forcing is not allowed. From top to bottom: 30 days, 60 days, 90 days assimilation window length with phase precision and without forcing adjustment.

crease from 100 %, 135 %, 62 % and 28 % to 73 %, 99 %, 32 % and 14 % for u, v, T and S, respectively (cf. Fig. 9 - 11, upper panels). The maximal horizontal mean improvements for u, v, T and S rise from 26 %, 20 %, 28 % and 25 % to 39 %, 23 %, 33 % and 27 %. Furthermore, the positive improvement pattern grow in size. The respective global mean SSH rms drops from 24 cm to 21 cm (compare Fig. 13 with Fig. 4). Still, the 30 days SHIFTASSIM cannot be considered as a good assimilation. The reproduction of variables in the 90 days SHIFTASSIM is further strengthened by more outer loops, too (Fig. 12, right panel). The mean SSH rms between TRUTH and 90 days SHIFTASSIM drop from 31 cm to 25 cm and become similar to the level of similarity the 30 days SHIFTASSIM shows with only one

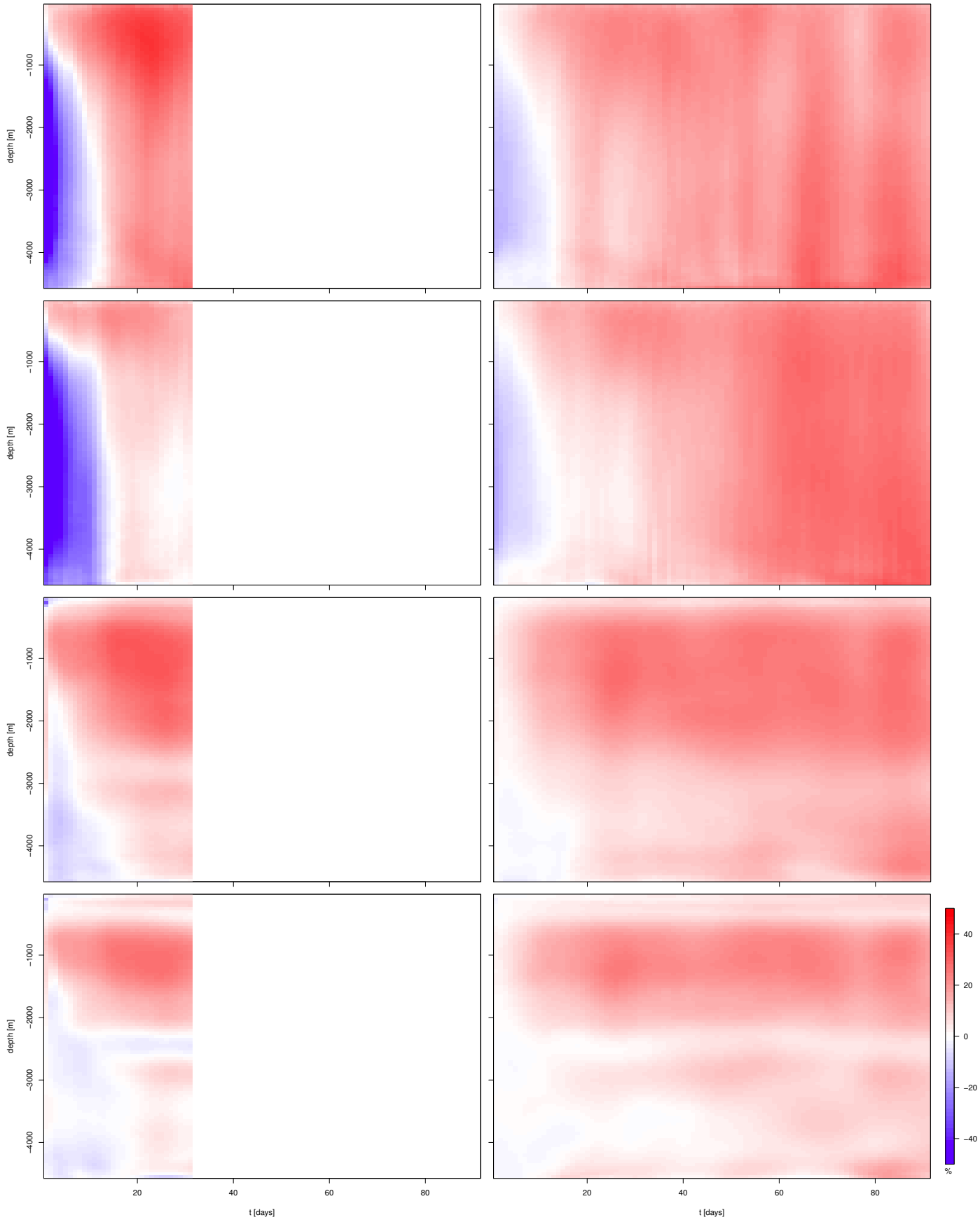

Fig. 12 Temporal development of the SSH assimilation impact on water mass properties after three outer loops. Differences between rms of SHIFTFREE and rms of SHIFTASSIM in relation to rms of SHIFTFREE. Positive values indicate a better reproduction of the respective TRUTH quantities in SHIFTASSIM than in SHIFTFREE. Negative values state the opposite. Horizontal mean for every time step and depth. Adaptation of the forcing is not allowed. Left panel: 30 days SHIFTASSIM. Right panel: 90 days SHIFTASSIM. From top to bottom: zonal velocity, meridional velocity, temperature, salinity.

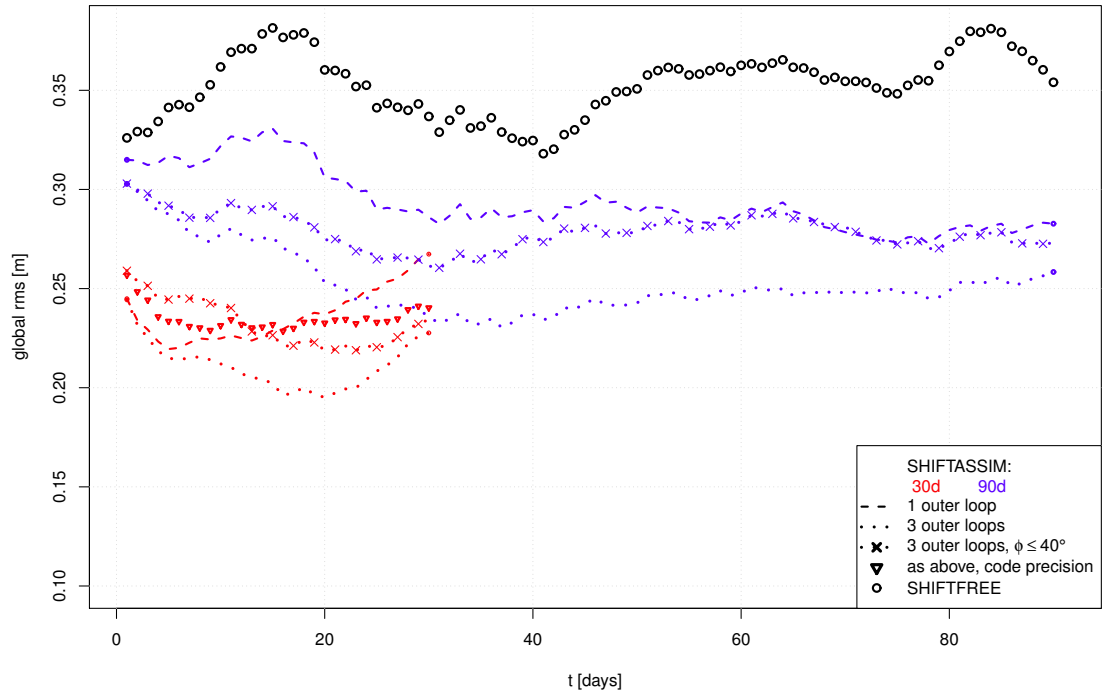

Fig. 13 Global mean rms misfits between SSH from SHIFTASSIM respectively SHIFTFREE and the true SSH (i.e., the noise-free SSH from TRUTH). Note, the SHIFTASSIM with one outer loop (the dashed lines) are the same as in Fig. 4).

outer loop (compare Fig. 13 with Fig. 4). As for the independent variables, the maximal horizontal mean improvements for u, v, T and S rise from 27 %, 33 %, 22 % and 19 % in the SHIFTASSIM with one outer loop to 35 %, 39 %, 29 % and 26 % in the SHIFTASSIM with three outer loops. Furthermore, the improvements cover a longer fraction of the assimilation time window (compare with Fig. 9 - 11, lower panels).

We conclude that the general characteristics of the respective SHIFTASSIM are not affected by the number of outer loops. Consequently, with three outer loops, the choice of phase or code precision for the observations has a minor impact on the results and the adaptation of forcings by the assimilation is still not advised (both not shown).

Independent of the number of outer loops, the window length dependency of the reproduction of sub-surface water mass properties is opposed to the dependency of the reproduction of the SSH which prefers short assimilation windows. We conclude that the longer assimilation windows provide more information about the internal state of TRUTH which is transferred from the observations into the ocean model and leads to a better reproduction of the entire original state after the assimilation.

To account for possible limitations of the space-borne GNSS-R measurements ,e.g., due to sea surface roughness (Semmling et al. 2014), some of the SHIFTASSIM have been repeated (c.f., Sec. 3) by using only observations with reflection incidence angles $\phi \leq 40^\circ$ (where $\phi = 0^\circ$ is perpendicular to the sea surface, i.e., zenith incidence). Because reflections from GPS satellites which are further away from the receiver are discarded, the observations follow the ISS ground track more closely (c.f., Fig. 1).

Consequently, this limitation results in a lower observation density (compare Fig. 14 with Fig. 2, left panels). Because of the altimetric sensitivity described in Sec. 2.3, the remaining SSH observations are those with the high precisions (compare Fig. 14 with Fig. 2, right panels). With these characteristics, the observations now share more similarities to SSH from conventional radar altimeters. Nonetheless, assimilating this high-quality but spatially sparse SSH data results in reduced performance compared to the full-observation SHIFTASSIM (see Fig 13). The global mean SSH rms misfits after 3 outer loops are 23 cm (28 cm) for the 30 (90) days ϕ-limited SHIFTASSIM. These rms are between the performances from 1 and 3 outer loops of the not-ϕ-limited 30 (90) days SHIFTASSIM which produced rms of 24 cm and 21 cm (31 cm and 25 cm).

The same is true for the recovery of the not assimilated quantities u, v, T and S (see Fig. 15). Both, the 30 and the 90 days ϕ-limited SHIFTASSIM with 3 outer loops perform less than the not-ϕ-limited SHIFTASSIM with 3 outer loops (compare with Fig. 12) but better than the respec-

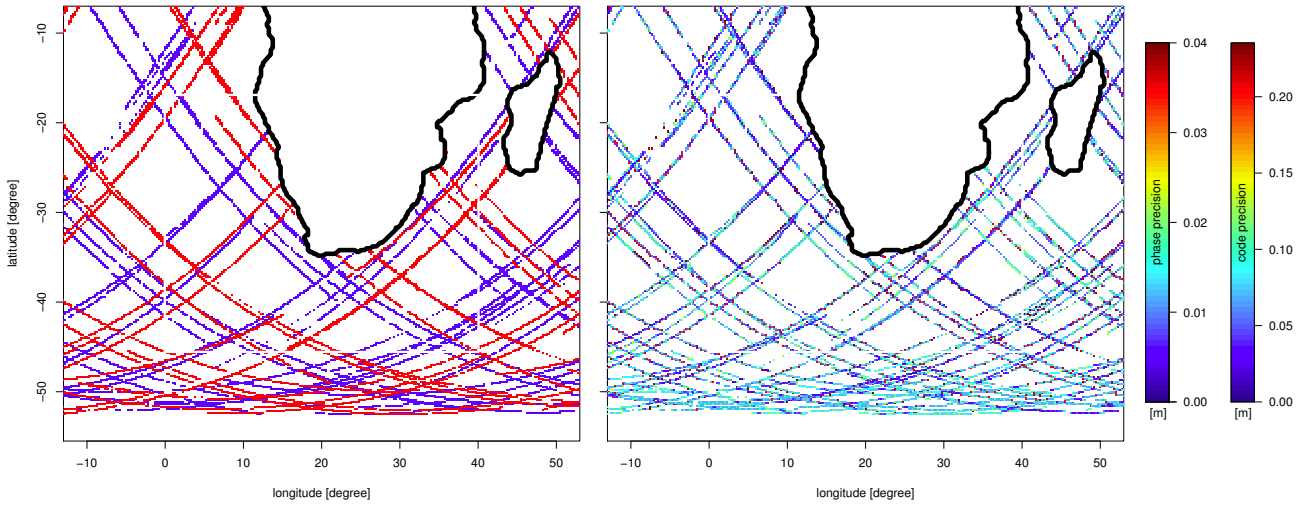

Fig. 14 Configuration of the artificial SSH observations by GNSS reflectometry when only $\phi \leq 40°$ are considered. GPS satellite reflection ground-tracks of two consecutive days (blue, red). Right: Precision at the respective grid-point, i.e., precision of the single measurements divided by the number of observations. Modelled SSH data is collected within the white rectangle only.

tive not-ϕ-limited SHIFTASSIM with 1 outer loop (compare with Fig. 9-11). The 3 outer loop ϕ-limited 90 days SHIFTASSIM can still be considered a physically consistent recovery but the maximal horizontal mean improvements for u, v, T and S are with 29 %, 21 %, 20 % and 22 % significantly smaller than the 35 %, 39 %, 29 % and 26 % from the respective not-ϕ-limited SHIFTASSIM.

Finally, a 3 outer loop ϕ-limited SHIFTASSIM was conducted that uses code precision instead of phase precision. The less precise ϕ-limited SSH observations result in a global mean SSH rms misfit of 24 cm for the 30 days SHIFTASSIM. This is a rise of 1 cm compared to the respective SHIFTASSIM which uses phase precision (see Fig. 13, triangles vs crosses). To a stronger extend the u, v, T and S reproduction is affected. For example, maximal horizontal mean improvements of the 30 day SHIFTASSIM for u, v, T and S change from 29 %, 28 %, 33 % and 28 % to 25 %, 19 %, 26 % and 29 % if code precision is used instead of phase precision. Note, the pattern of the respective reproductions remain very similar (not shown). We conclude that the reproduction of SSH, u, v, T and S in the ϕ-limited SHIFTASSIM depends on the choice of precision. This result is in contrast to the findings in the not-ϕ-limited SHIFTASSIM which are not significantly affected by the choice of precision. In the ϕ-limited SHIFTASSIM the reduced observation density results in a reduced ability of the assimilation method to compensate for the higher observation errors. Still, the impact of the observation errors on the performance of the assimilation is smaller than the impact of the observation density. We state that the information contained in large GNSS-R reflection angles is not redundant and can be recovered with advanced data assimilation methods. Consequently, the contained information should be used even when the respective observations have low precision. If for some reasons observations with large reflection angles are not usable then observations with phase precision are recommended (c.f., Semmling et al. 2014).

5 Summary

An idealized model based twin experiment is conducted to study the potential of sea surface height observations based on reflected signals from Global Navigation Satellite System satellites (GNSS-R) to determine internal water mass properties and transports of the Agulhas current system. A space-borne GNSS receiver is simulated on board of the International Space Station and resulting ground tracks and precisions of hypothetical SSH measurements are estimated. The single-receiver space-borne GNSS-R configuration already results in higher temporal and spatial coverage of the Earth but is accompanied by less precision compared to the conventional radar satellite altimetry. Based on an idealized GNSS-R configuration, daily SSH fields with 1-5° spatial resolution are possible. The precisions of a single SSH observation depends on reflection geometry and measurement method. If the carrier phase (code delay) information of the reflected GNSS signal is used, the precision can reach 3 cm (20 cm). The precision averaged over the studied Agulhas region is 7 cm (42 cm). The estimated ground tracks are used to sample modelled SSH from a general circulation model of the Agulhas current system. The estimated precision is accounted for by adding Gaussian noise to the sampled SSH. The resulting artificial SSH observations are assimilated into a different, i.e., six month shifted state of the same regional ocean model and the amount of recovery of the originally

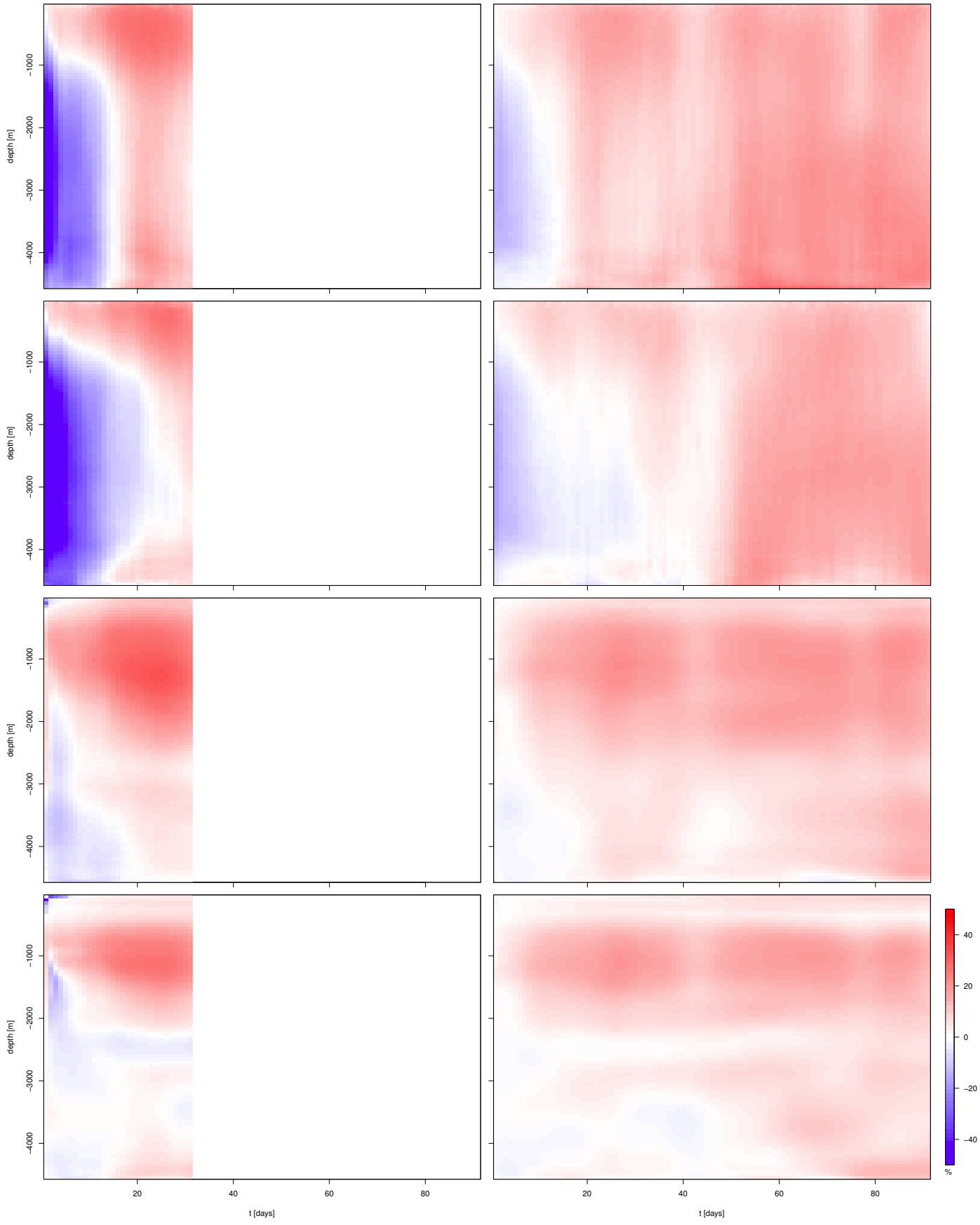

Fig. 15 Temporal development of the SSH assimilation impact on water mass properties after three outer loops and using only SSH observations with reflection incidence angle $\phi \leq 40°$. Differences between rms of SHIFTFREE and rms of SHIFTASSIM in relation to rms of SHIFTFREE. Positive values indicate a better reproduction of the respective TRUTH quantities in SHIFTASSIM than in SHIFTFREE. Negative values state the opposite. Horizontal mean for every time step and depth. Adaptation of the forcing is not allowed. Left panel: 30 days SHIFTASSIM. Right panel: 90 days SHIFTASSIM. From top to bottom: zonal velocity, meridional velocity, temperature, salinity.

observed state is quantized. A range of assimilation experiments is conducted which differ in window length (30 days to 90 days of assimilation), the control vector (with and without the adaptation of the atmospheric forcing), the utilized GNSS-R precision (phase or code precision) and the negligence of large reflection angles.

Not surprisingly, the assimilation of the noisy SSH results in an improved recovery of the original SSH as compared to the reference simulation. The recovery of the originally sampled SSH is best for the shortest assimilation window of 30 days. The mean rms differences decreases from 35 cm in the reference simulation to 21 cm in the assimilated simulations. The rms reduction is attributed to increased recovery of both, the mean SSH field and the temporal anomalies. The preference of the short assimilation window reflects the short system memory of the upper ocean. The recovery of the original SSH is also improved outside the assimilation region. The effect is most pronounced but not restricted to regions located down-stream of the assimilation area. The influence of the observation's precision in the range of code or phase precision is negligible. The respective precisions are not a limiting factor for the assimilation as long as all reflection angles are considered. The missing information is compensated by the dynamical ocean model in combination with the high temporal and spatial coverage of the GNSS-R data. The negligence of large reflection angles (more than 40° incidence angle) and the resulting lowering of the spatial observation density has a significant negative impact on the SSH recovery. The mean SSH rms differences rose from 21 cm to 23 cm. The inclusion of the atmospheric forcing into the OGCM's control vector has a small effect on the reproduction of the originally observed SSH but an unambiguous improvement cannot be reported. Ruling out the control by atmospheric forcing, the SSH observations are fitted by a changed initial model state.

The reproduction of internal water mass properties is studied by exploring the not assimilated quantities temperature, salinity and velocity during the assimilation time and throughout the entire water column. The quantities from the assimilation simulations are compared to the same quantities from the simulation the SSH are sampled from. In contrast to the reproduction of SSH, the independent quantities are closest reproduced in the longest assimilation window of 90 days. The 30 days assimilation is dominated by wrong values in the water mass properties leading to the conclusion that the corresponding good SSH reproduction is generated by wrong physical processes. The information of 60-90 days of observation is sufficient to distinguish the truly governing from the possible but not dominating physical processes. After 90 model days of data assimilation, up to 39 % of the original model state are recovered. As with the SSH recovery, the influences of observation's precision (code or phase) and the adaptation of atmospheric forcing on the internal water mass properties is small as long as all reflection angles are considered. In contrast to the SSH recovery, the inclusion of the atmospheric forcing into the assimilation's control vector leads to unambiguously worse results, i.e., the inclusion slightly dampens improvements and enhances wrong values in the sub-surface quantities. The adaptation of the wind forcing, if necessary, should be done with great caution and, if possible, be aided by additional observations, e.g., from ARGO floats or satellite gravimetry. Even more than for the SSH recovery, the negligence of the large reflection angles results in worse recovery of the internal water mass properties. The maximal recovery of the original state drops from 39 % to 29 %. In these experiments only, the choice of precision impacts the assimilation's performance to reproduce the internal water mass properties. Here, the reduced observation density is no longer able to fully compensate for the lesser precisions. Future GNSS-R satellite missions are well advised to consider SSH observations from large reflection incidence angles even when they are accompanied by small precision.

We conclude that assimilation of space-borne GNSS-R based SSH observations is a promising tool to constrain models of the Agulhas current system. The high temporal and spatial resolution of the GNSS-R observations compensate for the comparatively low precision of the measurements. Model estimates of deep water mass properties and transports improve significantly by assimilating daily SSH observations for at least 60 days. Longer assimilation windows, repeated or sequential assimilation are advised and will be explored in future studies. The outcome of our study should strengthen the consideration of oceanographic applications in near-future GNSS-R missions and guide their development. Real SSH data will be assimilated when space-borne GNSS-R observation become available. Furthermore, consistent studies combining the benefits of GNSS-R and conventional radar-altimetry are in preparation.

References

A. Albertella, R. Savcenko, T. Janji, R. Rummel, W. Bosch, J. Schröter, High resolution dynamic ocean topography in the Southern Ocean from GOCE. Geophys. J. Int. **190**, 922–930 (2012)

B.C. Backeberg, F. Counillon, J.A. Johannessen, M.I. Pujol, Assimilating along-track SLA data using the EnOI in an eddy resolving model of the Agulhas system. Ocean Dyn. **64**(8), 1121–1136 (2014)

L.M. Beal, W.P.M. De Ruijter, A. Biastoch, R. Zahn, On the role of the agulhas system in ocean circulation and climate. Nature **472**(7344), 429–436 (2011)

W. Bosch, R. Savcenko, D. Dettmering, C. Schwatke, *A Two-Decade Time Series of Eddy-resolving Dynamic Ocean Topography (iDOT)* (ESA/ESTEC, ???, 2012). ISBN 978-92-9221-274-2

E. Cardellach, A. Rius, A New Technique to Sense Non-Gaussian Features of the Sea Surface from L-Band Bi-Static GNSS Reflections. Rem. Sens. Environ. **112**, 2927–2937 (2008)

H. Carreno-Luengo, H. Park, A. Camps, F. Fabra, R. A., GNSS-R Derived Centimetric Sea Topography: An Airborne Experiment Demonstration. IEEE Sel. T. Appl. Earth Obs. Remote. Sens. **6**(3), 1468–1478 (2013)

G. Evensen, Inverse methods and data assimilation in nonlinear ocean models. Physica D **77**(1-3), 108–129 (1994)

V.O. Ivchenko, D. Sidorenko, S. Danilov, M. Losch, J. Schröter, Can sea surface height be used to estimate oceanic transport variability? Geophys. Res. Lett. **38** (2011)

A. Koutsodendris, J. Pross, R. Zahn, Exceptional agulhas leakage prolonged interglacial warmth during MIS 11c in europe. Paleoceanography **29**, 1062–1071 (2014)

J. Kuhlmann, H. Dobslaw, C. Petrick, M. Thomas, Ocean bottom pressure signals around southern africa from in situ measurements, satellite data, and modeling. J. Geophys. Res. **118**(10), 4889–4898 (2013)

D. Le Bars, J.V. Durgadoo, H.A. Dijkstra, A. Biastoch, W.P.M. De Ruijter, An observed 20-year time series of Agulhas leakage. Ocean Sci. **10**(4), 601–609 (2014)

F.X. Le Dimet, O. Talagrand, Variational algorithms for analysis and assimilation of meteorological observations - theoretical aspects. Tellus Ser. A-Dyn. Meteorol. Oceanol. **38**(2), 97–110 (1986)

S.T. Lowe, C. Zuffada, P. Chao Y. amd Kroger, L.E. Young, J.L. LaBrecque, 5-cm-precision aircraft ocean altimetry using GPS reflections. Geophys. Res. Lett. **29**(10), 1375–1378 (2002)

M. Martin-Neira, A passive reflectometry and interferometry system (PARIS): Application to ocean altimetry. ESA Journal **17**, 331–355 (1993)

A.M. Moore, H.G. Arango, G. Broquet, B.S. Powell, A.T. Weaver, J. Zavala-Garay, The Regional Ocean Modeling System (ROMS) 4-dimensional variational data assimilation systems Part I - System overview and formulation. Prog. Oceanogr. **91**(1), 34–49 (2011a)

A.M. Moore, H.G. Arango, G. Broquet, C. Edwards, M. Veneziani, B. Powell, D. Foley, J.D. Doyle, D. Costa, P. Robinson, The Regional Ocean Modeling System (ROMS) 4-dimensional variational data assimilation systems Part II - Performance and application to the California Current System. Prog. Oceanogr. **91**(1), 50–73 (2011b)

A.M. Moore, H.G. Arango, G. Broquet, C. Edwards, M. Veneziani, B. Powell, D. Foley, J.D. Doyle, D. Costa, P. Robinson, The Regional Ocean Modeling System (ROMS) 4-dimensional variational data assimilation systems Part III - Observation impact and observation sensitivity in the California Current System. Prog. Oceanogr. **91**(1), 74–94 (2011c)

G.S. Pilo, M.M. Mata, J.L.L. Azevedo, Eddy surface properties and propagation at southern hemisphere western boundary current systems. Ocean Sci. Discuss. **12**(1), 135–160 (2015)

M.-I. Pujol, G. Dibarboure, P.-Y. Le Traon, P. Klein, Using High-Resolution Altimetry to Observe Mesoscale Signals. J. Atmos. Ocean. Technol. **29**(9), 1409–1416 (2012)

A. Rius, E. Cardellach, M. Martin-Neira, Altimetric analysis of the sea surface GPS reflected signals. IEEE Trans. Geosci. Remote Sens. **48**, 2119–2127 (2010)

S. Ruehs, J.V. Durgadoo, E. Behrens, A. Biastoch, Advective timescales and pathways of agulhas leakage. Geophys. Res. Lett. **40**(15), 3997–4000 (2013)

G. Ruffini, F. Soulat, M. Caparrini, O. Germain, M. Martin-Neira, The eddy experiment: accurate gnss-r ocean altimetry from low altitude aircraft. Geophys. Res. Lett. **31**(L1230), 1–4 (2004)

v.E. Sebille, L.M. Beal, A. Biastoch, Sea surface slope as a proxy for Agulhas Current strength. Geophys. Res. Lett. **37** (2010)

A.M. Semmling, J. Beckheinrich, J. Wickert, G. Beyerle, S. Schön, F. Fabra, H. Pflug, K. He, J. Schwabe, M. Scheinert, Sea surface topography retrieved from gnss reflectometry phase data of the GEOHALO flight mission. Geophys. Res. Lett. **41**, 954–960 (2014)

M. Semmling, Altimetric Monitoring of Disko Bay using Interferometric GNSS Observations on L1 and L2, Technical report, 2012. doi:10.2312/GFZ.b103-12049

A.F. Shchepetkin, J.C. McWilliams, A method for computing horizontal pressure-gradient force in an oceanic model with a nonaligned vertical coordinate. J. Geophys. Res.-Oceans **108**(C3) (2003)

A.F. Shchepetkin, J.C. McWilliams, The regional oceanic modeling system (ROMS): a split-explicit, free-surface, topography-following-coordinate oceanic model. Ocean Model. **9**(4), 347–404 (2005)

M. Thomas, J. Sündermann, E. Maier-Reimer, Consideration of ocean tides in an OGCM and impacts on subseasonal to decadal polar motion excitation. Geophys. Res. Lett. **28**(12), 2457–2460 (2001)

S. Uppala, D. Dee, S. Kobayashi, P. Berrisford, A. Simmons, Toward a climate data assimilation system: Status update of ERA Interim, Technical report, ECMWF Newsl., 2008

W. Weijer, E. van Sebille, Impact of agulhas leakage on the atlantic overturning circulation in the ccsm4. J. Climate **27**(1), 101–110 (2014)

J. Wickert, G. Michalak, T. Schmidt, G. Beyerle, C.Z. Cheng, S.B. Healy, C.Y. Heise S. amd Huang, N. Jakowski, W. Köhler, C. Mayer, D. Offiler, E. Ozawa, A.G. Pavelyev, M. Rothacher, B. Tapley, , C. Arras, GPS radio occultation: Results from CHAMP, GRACE and FORMOSAT-3/COSMIC. Terr. Atmos. Ocean. Sci. **20**, 35–50 (2009)